

Direct observation of the coherent nuclear response after the absorption of a photon

M. Liebel, C. Schnedermann, G. Bassolino, G. Taylor,* A. Watts,* and P. Kukura†
Physical and Theoretical Chemistry Laboratory, South Parks Road, Oxford OX1 3QZ, UK

How molecules convert light energy to perform a specific transformation is a fundamental question in photophysics. Ultrafast spectroscopy reveals the kinetics associated with electronic energy flow, but little is known about how absorbed photon energy drives nuclear or electronic motion. Here, we used ultrabroadband transient absorption spectroscopy to monitor coherent vibrational energy flow after photoexcitation of the retinal chromophore. In the proton pump bacteriorhodopsin we observed coherent activation of hydrogen wagging and backbone torsional modes that were replaced by unreactive coordinates in the solution environment, concomitant with a deactivation of the reactive relaxation pathway.

The efficiency of light-induced processes fundamentally depends on the ability of a system to convert photons into chemical, electrical or mechanical energy. Resonance Raman intensity analysis reveals the initial energy distribution and the systems evolution over the first few tens of femtoseconds after photoexcitation [1, 2], while time-resolved optical spectra provide electronic kinetics. Neither of these techniques is capable of following the evolution of incident photon energy from the initially populated Franck-Condon (FC) region toward reactive rather than dissipative channels. It is this energy transfer, however, that is critical in determining the efficiency and outcome of a photo-induced process [3] and has been suggested to be subject to quantum coherent effects even for large protein assemblies at ambient condition [4–6].

The variation in reaction yields and speeds for retinal protonated Schiff base (RPSB) photoisomerization in different environments highlights the importance of the competition between active and passive relaxation pathways. In the proton pump bacteriorhodopsin (bR), excited state decay following photoexcitation is faster (0.5 vs 4 ps) [7, 8], results in a higher isomerization yield (0.64 vs 0.16) [9, 10] and produces exclusively the 13-*cis* rather than the 11-*cis* isomer formed in solution. Nevertheless, the resonance Raman spectra of both RPSBs are strikingly similar [11] implying an essentially identical starting geometry and initial structural evolution. Raman active totally symmetric stretching coordinates, however, cannot contribute to the formation of a conical intersection between states of opposite symmetry and thus to efficient electronic relaxation [12].

The reactivities observed for RPSB in solution compared to the protein environment must therefore result from the activation of different nuclear motions by energy transfer from the initially populated coordinates. To reveal the energy flow, we created and followed vibrational coherence with specific sensitivity to the region near the vibronic surface crossing using impulsive vibrational spectroscopy [13]. Illustrating this experimental approach with RPSB, absorption of an ultrashort visible photon generates vibrational coherence in all nuclear degrees of freedom coupled to the optical transition in both

ground (S_0) and excited (S_1) electronic states (FIG. 1) [14]. The impulsively created S_0 nuclear wavepacket oscillates about its equilibrium position whereas on S_1 it rapidly moves out of the FC region toward a new stationary point (SP) [15]. At this local minimum, the backbone structure has evolved little along the isomerization coordinate and experiences a barrier toward excited state decay [16, 17]. Previous attempts to reveal reactive nuclear wavepacket evolution [18] have struggled either with interfering ground state signatures [19, 20] or insufficient time-resolution revealing only low-frequency coherences [21]. As a result, only limited insight into the reactive dynamics from the perspective of a few degrees of freedom was available.

Here, we combined high time resolution transient absorption spectroscopy with ultrabroad (500 - 900 nm) detection bandwidth, spectroscopic sensitivity ($<10 \mu\text{OD}$) and electronic population control to conclusively reveal excited state nuclear wavepacket dynamics over the full spectral window of interest ($<2000 \text{ cm}^{-1}$).

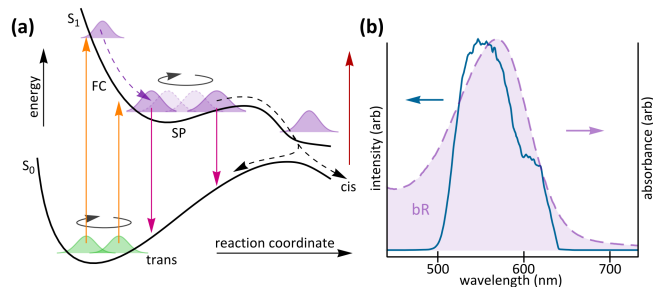


FIG. 1. Schematic potential energy diagram for retinal isomerization and excitation conditions. (a) Potential energy of the ground (S_0) and excited (S_1) electronic states of RPSB along the isomerization coordinate including nuclear wavepacket dynamics. FC: Franck-Condon region; SP: stationary point. (b) Overlay of the 9.6 fs excitation pulse (solid) with the bacteriorhodopsin absorption spectrum (dashed).

The differential absorbance map of RPSB in bR after optical excitation with a <10 fs pulse is shown in FIG. 2a. Early time-delays (<100 fs) are dominated by the coherent artifact caused by the interaction of pump

and probe pulses with the sample [22], rapidly followed by ground state bleach (570 nm) and stimulated emission bands (>750 nm). Both signatures decay with the characteristic excited state lifetime of 0.5 ps concomitant with a growth of the photoproduct absorption band at 640 nm. Given the high time-resolution (<20 fs) achieved in this work, the broad and slowly varying spectral and temporal electronic features are complemented by rapid oscillations caused by the impulsively excited nuclear wavepackets (see FIG. 1a).

Subtraction of the exponential electronic kinetics reveals the pure vibrational coherence, including two phase jumps, one at slightly lower energy than the S_0 absorption maximum (580 nm) and another at the border between ground and excited state signatures (750 nm) (FIG. 2b). The near-infrared (NIR) coherence is strongly damped compared to the one observed in the S_0 absorption window (<650 nm), in agreement with the short S_1 lifetime (0.5 ps). These observations suggest that the visible region is dominated by nuclear coherence on S_0 , while the NIR mainly exhibits signatures caused by vibrational wavepackets evolving on S_1 .

To conclusively remove any residual S_0 coherences in the NIR, we determined the frequencies and dephasing times of all contributing oscillations using a combination of linear prediction singular value decomposition [23] and nonlinear optimization. A sum of 24 exponentially decaying oscillations was sufficient to describe the observed coherence decay to within the measurement noise (FIG. 2c inset) and revealed the presence of some coherences with dephasing times exceeding 0.45 ps, all of which showed frequencies matching known S_0 bands, such as the C=C band at 1526 cm^{-1} .

After removal of these S_0 signatures we are left with a spectrum representative of coherence activity on S_1 only exhibiting a completely altered intensity and frequency distribution compared to the S_0 frequency-domain Raman spectrum of bR (FIG. 2c). The hydrogen wag at 952 cm^{-1} dominates the spectrum, with lesser contributions from additional wagging (900 cm^{-1}), Schiff base (1075 cm^{-1}) and backbone torsional (177 cm^{-1}) coordinates. Recent coherent infrared emission spectra on bR agree with our observations of strong activity in the 750-1150 cm^{-1} region, but an unambiguous assignment of the observed features was hampered by numerous additional modes of unknown origin [24].

An important consequence of our detection methodology is that vibrational motion which strongly modifies the S_0 - S_1 energy gap will also generate the most prominent oscillatory features in the transient electronic spectra (FIG. 1a). Given that the critical step during the isomerization reaction is the passage from S_1 to S_0 through a conical intersection, the most active modes in our experiment are likely to be the strongest contributors to excited state decay and thus the photoisomerization. Despite the complexity of the system with more than 300

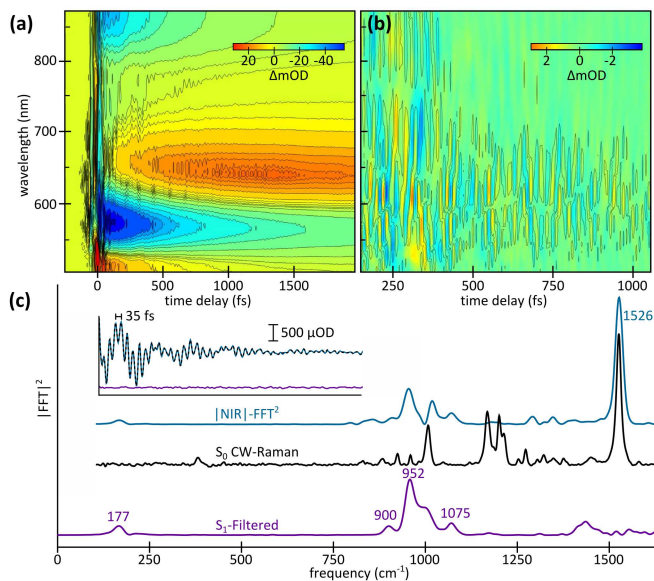


FIG. 2. Reactive nuclear wavepacket dynamics during retinal isomerization in bacteriorhodopsin (bR). (a) Chirp corrected [25] differential absorbance map of bR after resonant excitation by a 9.6 fs pulse (FIG. 1b). The sample was flown through a sample cell at $\text{OD} = 0.45/500$ μm . Pump and probe intensities were adjusted to be 200 and 2.5 nJ at a laser repetition rate of 2 kHz with 100 and 60 μm beam diameters, respectively. (b) Residual vibrational coherence map after global subtraction of the exponential electronic kinetics [26]. The contour lines shown were limited to the 800 - 1200 cm^{-1} frequency window for clarity. (c) Fourier power spectrum of the coherence after application of a Kaiser window before and after removal of long-lived (>0.45 ps dephasing time) coherences and comparison to S_0 Raman spectrum. The peak intensities were corrected for the limited time-resolution. Inset: wavelength averaged (760-840 nm) coherent activity of b, fit to 24 exponentially decaying oscillations.

nuclear degrees of freedom, the S_1 vibrational coherence of RPSB in bR is dominated by the hydrogen wag at 952 cm^{-1} , a motion essential to C=C isomerizations [27] and capable of coupling the ground and excited electronic states potential energy surfaces (PES). The results presented in FIG. 2c thus suggest a correspondence between the ability of a systems to focus energy into a few critical coordinates and the photochemical outcome of excited state decay.

Although such an interpretation is appealing, it does not prove a correlation between the observed nuclear coherence, the shape of the PES and photochemical reactivity. By synthesizing a series of RPSBs with different Schiff bases, we found that using p-methoxyaniline (pma) as a base completely eliminated all isomerizing channels (FIG. 3a). The close resemblance of the S_0 Raman spectrum of pma-RPSB to that of RPSB in bR (see FIG. 2c) suggests similar ground state geometries, excited electronic state character and initial nuclear evolution for RPSB in bR and pma-RPSB in solution. In contrast to

RPSB in bR, however, the S_1 coherence shows negligible activity in the hydrogen wagging ($<1000\text{ cm}^{-1}$) and torsional ($<300\text{ cm}^{-1}$) regions of the spectrum and is instead dominated by stretching coordinates with significant contributions likely originating from the aromatic Schiff base moiety ($1000\text{-}1300\text{ cm}^{-1}$), as verified by comparison with fully deuterated pma (FIG. 3b).

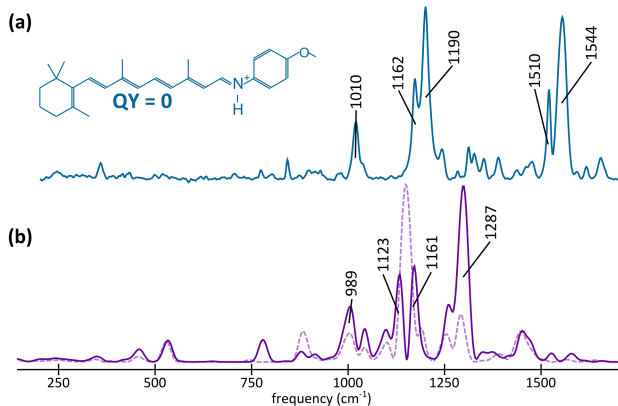


FIG. 3. Comparison of ground and excited state Raman activity in p-methoxyaniline RPSB (pma-RPSB). (a) Molecular structure of pma-RPSB and ground state frequency-domain Raman spectrum recorded in acetonitrile. (b) Fourier power spectrum of photon-induced excited state vibrational coherence of pma-RPSB (solid) and fully deuterated pma-RPSB (dashed) averaged over the 760 - 850 nm spectral window measured analogous to RPSB in bR using a resonant 6.8 fs pulse. For pma-RPSB, no removal of residual ground state coherences as for RPSB in bR was possible, but the dramatically different appearance of the ground and excited state spectra suggests minor contributions from residual S_0 coherences.

In contrast to most current ultrafast techniques, the vibrational coherence presented in this work was generated by the photon that triggers the light induced process. Our results thus do not simply report on the structural evolution of the molecule of interest, but instead on the coherent vibrational energy flow along the S_1 PES out of the FC region during the isomerization reaction. Based on the S_0 Raman spectra, we would have expected strong coherent activity in backbone stretches for RPSB in bR and in solution, but observed exactly the opposite experimentally. In fact, given that S_1 vibrational coherence is generated mainly in FC active modes, we would expect the power spectra of S_1 coherent activity to be as similar as the respective S_0 Raman spectra.

The dramatically different appearance of the S_0 and S_1 spectra cannot be solely attributed to vibrational structural changes caused by different bonding properties upon electronic excitation. The apparent lack of backbone stretching activity in bR is *a priori* surprising, given the dominant presence of C=C stretching modes in the Raman spectra of polyenic systems. Such behaviour, however, has been previously observed in the photoiso-

merization of stilbene [28]. Here, totally symmetric coordinates remain dominant in the Raman spectrum of the excited electronic state for the *trans*-isomer but disappear almost completely for the more reactive *cis*-isomer likely due to significant symmetry changes caused by molecular distortion. The key question thus relates to the mechanism by which vibrational coherence can appear in initially silent and disappear from initially excited degrees of freedom. The latter can be explained by a change in equilibrium displacement between S_0 and S_1 as the structure of the molecule evolves on the excited electronic state. The former, however, must be related to the shape of the PES away from the FC region [3].

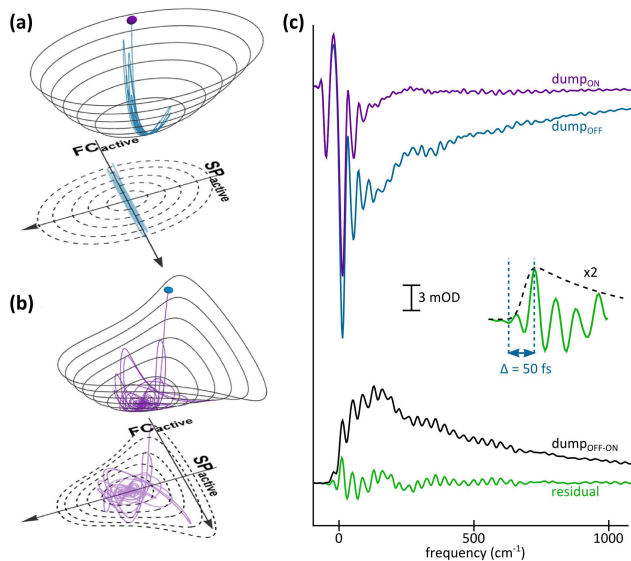


FIG. 4. Anharmonic coupling mediates coherent activation of hydrogen wagging on the <50 fs timescale. (a) Potential energy surface and classical trajectory for two uncoupled nuclear coordinates, with only one coordinate being significantly displaced with respect to the ground electronic state. (b) PES and dynamic evolution for identical initial displacements as in a, but with the addition of a strong anharmonic coupling term. (c) Recording of the differential absorption in the 760-840 nm spectral region in the presence and absence of a ps dump pulse resonant only with the $S_0 \leftarrow S_1$ transition removes the coherent artifact around zero time delay and reveals the rapid rise of the coherent vibrational activity. Inset: Magnification of the rising coherence amplitude.

Consider a simplified, two-dimensional excited state PES consisting of two uncoupled nuclear coordinates, only one of which is displaced from its equilibrium position in the FC region. For a $\pi^* \leftarrow \pi$ excitation, two such coordinates may be the symmetric C=C stretch and an asymmetric hydrogen wag. Upon population of S_1 , the system oscillates along the displaced stretching coordinate about its new equilibrium bond length but without gaining any momentum along the initially silent asymmetric wag (FIG. 4a). By introducing a coupling term between the two modes this behavior changes drastically.

The system now gains momentum along the asymmetric coordinate after the first tens of fs, even if the initial displacement was close to zero (FIG. 4b). Such a shift, however, does not necessarily induce significant changes in the resonance Raman spectra, because only the earliest dynamics are sampled [2].

To quantify the timescale for the coherent vibrational coupling process, we used electronic population control to eliminate the otherwise dominant coherent artifact around time-zero, thus revealing the full temporal evolution of the vibrational coherence down to the earliest time-delays. Using a long (1 ps) dump pulse centered at 880 nm, we selectively removed S_1 population without impulsively generating additional nuclear wavepackets or affecting the S_0 population. By subtracting the transient dynamics in the absence and presence of the dump pulse we removed the coherent artifact and revealed the rapid rise of the vibrational coherence on the sub 50 fs timescale (FIG. 4c). Interestingly, this growth is comparable to the recently reported rise time of the SE signal and matches the kinetics of tentatively assigned excited state signatures at wavelengths $>1 \mu\text{m}$ [16, 21]. The major changes responsible for the observed vibrational coherence transfer does take place during the first tens of femtoseconds after photoexcitation.

In conclusion, we used ultrabroadband transient absorption spectroscopy with high temporal resolution to reveal the coherent nuclear response of a molecule after absorption of a photon. In contrast to the expectation that the photon-induced structural evolution largely takes place along FC active coordinates, we observed efficient and coherent activation of initially silent vibrational modes caused by PES-induced anharmonic coupling. We further demonstrated that the nature of the coherent evolution differs dramatically with the environment of the molecule and is strongly correlated with the efficiency and outcome of the light induced process as evidenced by the comparison of RPSB in bR and pma-RPSB in solution. Interestingly, the coherent evolution takes place on the <50 fs timescale, fast enough to allow for quantum coherent effects to remain active and decisive for the eventual outcome of the process [29], irrespective of the photoexcitation mechanism. Our results emphasize the importance of ultrafast energy flow in determining the outcome of light-induced processes and demonstrate the power of vibrational spectroscopy in the time-domain for studying the structural and dynamic origins of molecular relaxation phenomena.

* Department of Biochemistry, Biomembrane Structure Unit, University of Oxford, Oxford, OX1 3QU, United Kingdom.

- † philipp.kukura@chem.ox.ac.uk
- [1] A. Warshel, *Annu. Rev. Biophys. Bio.* **6**, 273 (1977).
 - [2] E. J. Heller, *Accounts Chem. Res.* **14**, 368 (1981).
 - [3] S. Takeuchi, S. Ruhman, T. Tsuneda, M. Chiba, T. Taketsugu, and T. Tahara, *Science* **322**, 1073 (2008).
 - [4] Q. Wang, R. W. Schoenlein, L. A. Peteanu, R. A. Mathies, and C. V. Shank, *Science* **266**, 422 (1994).
 - [5] G. S. Engel, T. R. Calhoun, E. L. Read, T.-K. Ahn, T. Mancal, Y.-C. Cheng, R. E. Blankenship, and G. R. Fleming, *Nature* **446**, 782 (2007).
 - [6] E. Collini, C. Y. Wong, K. E. Wilk, P. M. G. Curmi, P. Brumer, and G. D. Scholes, *Nature* **463**, 644 (2010).
 - [7] R. A. Mathies, C. H. Brito Cruz, W. T. Pollard, and C. V. Shank, *Science* **240**, 777 (1988).
 - [8] H. Kandori and H. Sasabe, *Chem. Phys. Lett.* **216**, 126 (1993).
 - [9] J. Tittor and D. Oesterhelt, *FEBS Lett.* **263**, 269 (1990).
 - [10] K. A. Freedman and R. S. Becker, *J. Am. Chem. Soc.* **108**, 1245 (1986).
 - [11] S. O. Smith, M. S. Braiman, A. B. Myers, J. A. Pardoen, J. M. L. Courtin, C. Winkel, J. Lugtenburg, and M. A. Richard, *J. Am. Chem. Soc.* **109**, 3108 (1987).
 - [12] B. G. Levine and T. J. Martínez, *Annu. Rev. Phys. Chem.* **58**, 613 (2007).
 - [13] H. L. Fragnito, J.-Y. Bigot, P. C. Becker, and C. V. Shank, *Chem. Phys. Lett.* **160**, 101 (1989).
 - [14] W. T. Pollard and R. A. Mathies, *Annu. Rev. Phys. Chem.* **43**, 497 (1992).
 - [15] M. Garavelli, P. Celani, F. Bernardi, M. Robb, and M. Olivucci, *J. Am. Chem. Soc.* **119**, 6891 (1997).
 - [16] K. C. Hasson, F. Gai, and P. A. Anfirud, *P. Natl. Acad. Sci. USA* **93**, 15124 (1996).
 - [17] S. Ruhman, B. Hou, N. Friedman, M. Ottolenghi, and M. Sheves, *J. Am. Chem. Soc.* **124**, 8854 (2002).
 - [18] T. Kobayashi, T. Saito, and H. Ohtani, *Nature* **414**, 531 (2001).
 - [19] S. L. Dexheimer, Q. Wang, L. A. Peteanu, W. T. Pollard, R. A. Mathies, and C. V. Shank, *Chem. Phys. Lett.* **188**, 61 (1992).
 - [20] J. P. Kraack, T. Buckup, and M. Motzkus, *Phys. Chem. Chem. Phys.* **13**, 21402 (2011).
 - [21] A. Wand, B. Loevsky, N. Friedman, M. Sheves, and S. Ruhman, *J. Phys. Chem. B* **117**, 4670 (2012).
 - [22] A. L. Dobryakov, S. A. Kovalenko, and N. P. Ernsting, *J. Chem. Phys.* **123**, 044502 (2005).
 - [23] A. E. Johnson and A. B. Myers, *J. Chem. Phys.* **104**, 2497 (1996).
 - [24] G. I. Groma, A. Colonna, J.-L. Martin, and M. H. Vos, *Biophys. J.* **100**, 1578 (2011).
 - [25] S. A. Kovalenko, A. L. Dobryakov, J. Ruthmann, and N. P. Ernsting, *Phys. Rev. A* **59**, 2369 (1999).
 - [26] M. Liebel and P. Kukura, *J. Phys. Chem. Lett.* **4**, 1358 (2013).
 - [27] P. Kukura, D. W. McCamant, S. Yoon, D. B. Wand-schneider, and R. A. Mathies, *Science* **310**, 1006 (2005).
 - [28] A. L. Dobryakov, I. Ioffe, A. A. Granovsky, N. P. Ernsting, and S. A. Kovalenko, *J. Chem. Phys.* **137**, 244505 (2012).
 - [29] V. I. Prokhorenko, A. M. Nagy, S. A. Waschuk, L. S. Brown, R. R. Birge, and R. J. D. Miller, *Science* **313**, 1257 (2006).